Aalborg Universitet

AALBORG UNIVERSITY

General Unified Integral Controller with Zero Steady-State Error for Single-Phase Grid-Connected Inverters

Guo, Xiaoqiang; Guerrero, Josep M.

Link to publication from Aalborg University

General Unified Integral Controller with Zero Steady-State Error for Single-Phase Grid-Connected Inverters

Xiaoqiang Guo, *Senior Member, IEEE,* and Josep M. Guerrero, *Fellow, IEEE*

Abstract—**Current regulation is crucial for operating single-phase grid-connected inverters. The challenge of the current controller is how to fast and precisely tracks the current with zero steady-state error. This paper proposes a novel feedback mechanism for the conventional PI controller. It allows the steady-state error suppression with no need of additional complex control algorithms such as the synchronous reference frame transformation. Five alternative implementation methods are comparatively evaluated from the viewpoint of the steady-state and dynamic responses. Further, the theoretical analysis done indicates that the widely used PR (P+Resonant) control is just a special case of the proposed control solution. The time-domain simulation in Matlab/Simulink and experimental results from a TMS320F2812 DSP based laboratory prototypes are in good agreement, which verify the effectiveness of the proposed generalized method.**

Keywords- Grid-connected inverter, general unified integral controller, zero steady-state error control

I. INTRODUCTION

The environmental concerns and electric utility deregulation promote the development of distributed generation and microgrid in a rapid pace [1-7]. These systems using renewable energy sources (RES) have many advantages such as the on-site power production for the local loads. Consequently, the losses of long power transmission lines can be significantly reduced. Typically, a voltage-source current-regulated inverter is used for the power flow control of RES systems [8-11]. One of the most important issues is how to fast and precisely track the current of the grid-connected inverters, trying to avoid the steady-state error.

Many current control techniques have been presented in the past decades, such as hysteresis control [12], [13], one cycle control [14], predictive control [15], [16], Lyapunov-based control [17]. Among them, the proportional integral (PI) control is a simple and widely-used solution. However, it has the disadvantage of having steady-state amplitude and

---

phase errors. By using the synchronous rotating frame, the PI

regulator can eliminate the steady-state error associated with stationary frame PI regulators. Nevertheless, it cannot be applied to single-phase systems in a straightforward way. In order to overcome this limitation, some alternative solutions have been presented in [18-20], which uses a 90 degrees delayed signal, the Hilbert transformation, or an all pass filter in order to reconstruct a *virtual* three-phase system. In this way, it is feasible to obtain a two-phase quadrature signals, similar as a synchronous rotating frame, thus can be possible to apply a conventional PI for each direct and quadrature (*d-q*) components to achieve the zero steady-state error. The reason of this fact is that d-q components are constant values in steady state. So that PI control can track well those values. Another interesting approach has been reported in [21], which reconstructs the 90-degree phase-shift component from the capacitor voltage and current, instead of the signal delay. However, the abovementioned PI-based solutions require many rotating frame transformations, thus increasing the implementation complexity.

The objective of this paper is to develop an enhanced PI control, which integrates PI control with a simple feedback term to eliminate the steady-state error with no need of additional complex algorithms such as the synchronous reference frame transformations. It has a very simple structure and can be easily implemented in practical applications. In addition, the resonant frequency of the controller is easy to adjust. This is especially attractive for applications like frequency droop controlled MicroGrids, in which the frequency is changed according to the active power participation of each inverter. That means that the output frequency reference of the inverter can change the fundamental and harmonics resonant frequencies of their respective controllers [1]. Other applications can be active power filters, uninterruptible power supplies, and so on.

The paper is organized as follows. Section II presents a brief review of the conventional three- and single-phase synchronous reference frame control strategy. Section III presents the proposed control strategy. Section IV evaluates the performance of the proposed general unified integral controller. Finally, conclusions are provided in Section IV.

II. SYNCHRONOUS REFERENCE FRAME CONTROL

This section will provide a brief review of the three-phase and single-phase synchronous reference frame (SRF) control strategy.

A. Three-phase SRF Control Scheme

It is well known that zero steady-state error control of a dc value can be easily achieved by a PI regulator. However, for an ac value, the steady-state error can not be eliminated with PI regulator, and the error will depend, among others, on the frequency of the ac value.

In practical applications, there are many ac quantities such as the sinusoidal voltage and current signals. By transforming the time-varying ac signal with the synchronous reference frame transformation, the ac quantity will become dc signal. In that case, the steady-state error can be eliminated by a PI regulator in spite of the frequency of ac sinusoidal signal to be tracked.

Fig. 1 illustrates the block diagram of the conventional three-phase SRF control strategy. First of all, the error (x_{abc}) of three-phase ac quantities is transformed into dc quantities with the synchronous reference frame transformation, and then the steady-state error can be easily eliminated by using the integral-based regulator. Finally, the results are transformed back to the stationary frame. Note that, the proportional regulator can be used in either synchronous reference frame or stationary frame in order to enhance the system dynamic response.
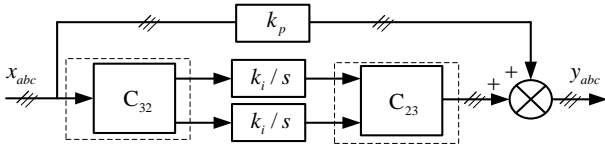

Fig. 1. Three-phase SRF control scheme

B. Single-phase SRF Control Scheme withVirtual Three-Phase Signal Reconstruction

Three-phase SRF control strategy has been widely used in many industrial applications due to its high control accuracy. This approach can also be used in single-phase applications. Indeed, the single-phase ac quantity can be considered as a special case of three-phase unbalanced ac quantities. More specifically, only one phase is considered, while the other two are neglected, as shown in Fig. 2.
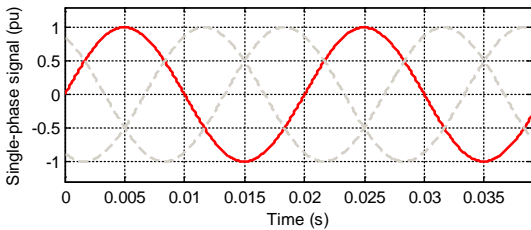

Fig. 2. Virtual three-phase unbalanced ac signals

Therefore, from the theoretical point of view, it seems that three-phase SRF control strategy can be also applied to single-phase applications. However, a special modification of the SRF control strategy should be made to cope with the negative sequence component, which is resulted from the unbalance of the *virtual* three-phase ac signals. A possible solution is to use the dual SRF control strategy reported in [22]. However, it needs many synchronous reference frame transformations, making its implementation more complex.

In order to avoid many SRF transformations and to simplify the control strategy, many other interesting solutions have been reported. The basic idea is to reconstruct

the *virtual* three-phase (or the two-phase quadrature) ac signals from the single-phase ac signal, named Signal Reconstruction (SR) block.

An intuitive solution to construct a *virtual* three-phase signal is to delay 120 and 240 degrees the single-phase ac signal, as shown in Fig. 4 (a). In this way, the conventional three-phase SRF control strategy of Fig. 1 can be applied, as shown in Fig. 3.
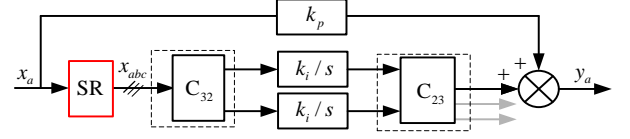
Fig. 3. Single-phase SRF control scheme with virtual abc frame

(a)

(b)
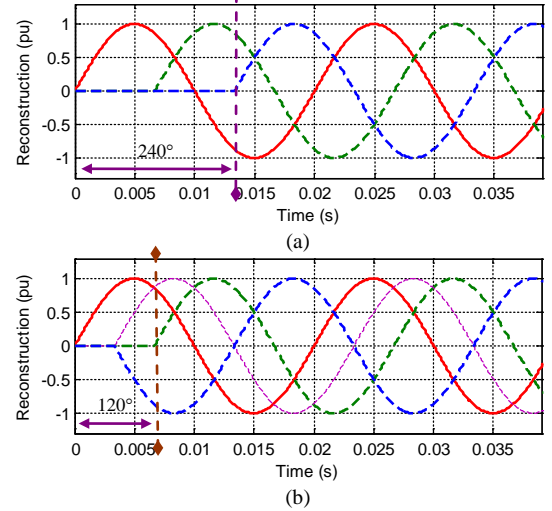
Fig. 4. Signal reconstruction with virtual *abc frame*

It should be noted that this construction process needs a delay of 2/3 fundamental period. Much delay might endanger the system stability. One possible solution is to delay the single-phase ac quantity by 120 and 60 electrical degrees, and then reverse the 60-degrees-delayed signal, as shown in Fig. 4 (b). In this way, the maximum delay can be reduced from 2/3 cycle (240 degrees) to 1/3 cycle (120 degrees).

C. Single-phase SRF Control Scheme in Virtual Two-Phase Signal Reconstruction

In order to further reduce the delay and simplify the control strategy, another interesting solution has been reported in [18]. The basic idea is to reconstruct *virtual* two-phase quadrature ac signals by delaying the delay the single-phase ac signal by 90 electrical degrees, as shown in Fig. 5.

Fig. 5. Signal reconstruction with virtual $\alpha\beta$ *frame*

In this way, the maximum delay can be reduced from 2/3 cycle (240 degrees) to 1/4 cycle (90 degrees). Then, the conventional three-phase SRF control strategy of Fig. 1 can be applied, as shown in Fig. 6.

Fig. 6. Single-phase SRF control scheme with virtual $\alpha\beta$ frame
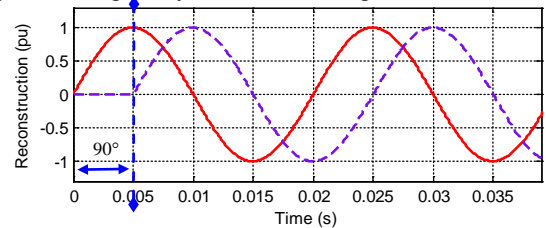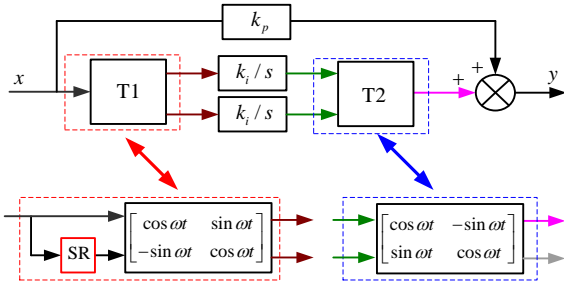
III. PROPOSED CONTROLLER

As discussed in the previous Section, the SRF control strategy can be extended to single-phase applications with zero-steady-steady error, thanks to the signal reconstruction (SR) block. It might be a good solution from a theoretical point of view. However, it still needs many synchronous reference frame transformations, which inevitably increase the computational burden.

In order to solve the abovementioned problem, a general unified integral controller is proposed. It is similar to the PI controller, except for a simple feedback path. The basic diagram of proposed control is illustrated in Fig. 7.
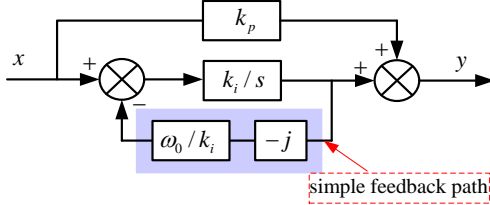

Fig. 7. Basic diagram of proposed control method

The transfer function in Fig. 7 is given in (1). It can achieve the zero steady-state error control of both dc and ac components. That is the reason we call it the general unified integral controller.

$$C(s) = \frac{M(s)}{s - j\omega_0} = \frac{k_p s + k_i - jk_p \omega_0}{s - j\omega_0} \quad (1)$$

For example, when the control variable is a 0Hz dc component, the coefficient ω_0 in (1) is set to 0. That is, equation (1) becomes the classical proportional integral controller. And it is well known that PI controller can achieve the zero steady-state error control of dc components.

On the other hand, if the control variable is a 50Hz ac component, the coefficient ω_0 in (1) is set to 100π to achieve the zero steady-state error control of the fundamental frequency component. In the same way, the coefficient ω_0 can be set to other values to accurately control the harmonic fundamentals as well.

A. *Case study*

Fig. 8 shows the schematic diagram of a typical single-phase grid-connected inverter, which is an illustrative example to test the control proposal. Note that, following will focus on the current control, while other issues such as the maximum power point tracking, anti-islanding protection, grid synchronization and leakage current suppression [23-26] are out of scope of this paper.
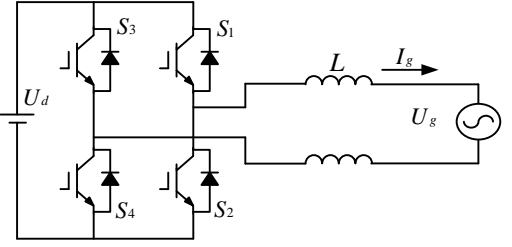
Fig. 8. Diagram of single-phase grid-connected inverter

Assuming that the switching frequency is high enough to neglect the inverter dynamics, the equivalent representation of the single-phase current regulated grid-connected inverter is obtained as shown in Fig. 9, where $C(s)$ is the current regulator transfer function, K is the PWM gain, T_d is the control delay, and L and R are the filter inductor and its equivalent series resistor.
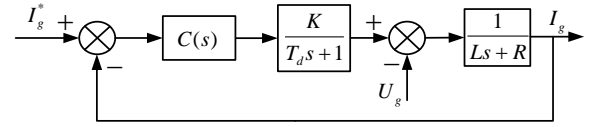
Fig.9. Linear control model of single-phase grid-connected inverter

The system closed-loop transfer function can be derived from Fig. 9 as follows:

$$I_g(s) = \frac{KC(s)}{LT_d s^2 + (RT_d + L)s + R + KC(s)} I_g^*(s)$$
$$- \frac{T_d s + 1}{LT_d s^2 + (RT_d + L)s + R + KC(s)} U_g(s) \quad (2)$$

Equation (2) indicates that the grid current $I_g(s)$ is dependent on the current reference $I_g^*(s)$ and the grid voltage $U_g(s)$, which can be seen as a disturbance here.

By substituting (1) into (2), the system closed-loop transfer function can be expressed as follows:

$$I_g = \overbrace{\frac{KM(s)}{[LT_d s^2 + (RT_d + L)s + R](s - j\omega_0) + KM(s)}}^{A(s)} I_g^*(s)$$
$$- \overbrace{\frac{(s - j\omega_0)(T_d s + 1)}{[LT_d s^2 + (RT_d + L)s + R](s - j\omega_0) + KM(s)}}^{B(s)} U_g(s)$$
(3)

From (3), we can obtain that the terms $A(s)=1$ and $B(s)=0$ when the angular frequency of the reference $I_g^*(s)$ and the disturbance $U_g(s)$ are equal to ω_0. That is to say, the regulated grid current $I_g(j\omega_0)$ perfectly tracks its reference. So that, zero steady-state error current regulation is achieved.

B. *Parameter Tuning*

This section will provide a practical tuning method for the controller parameters. Traditionally, in a PI control the higher is the control bandwidth, the better are the steady-state and dynamic responses. Nevertheless, in practice the high bandwidth usually leads to instability due to the control delay, especially in digital control applications [27]. A practical way to avoid instability is to keep the control bandwidth below one fifth of the sample frequency. For example, the control bandwidth is selected below 2 kHz with the sample frequency of 10 kHz.

For simplicity, the ESR and control delay T_d are neglected due to their small values. The system magnitude-frequency function can be derived from (1) and (2) as follows:

$$|T_1(s)| = \frac{K\sqrt{k_i^2 + k_p^2(\omega - \omega_0)^2}}{\sqrt{(L\omega\omega_0 - L\omega^2 + Kk_i)^2 + (Kk_p)^2(\omega - \omega_0)^2}} \quad (4)$$

The following steps are proposed in order to select properly the main control parameters.

Step 1. Assuming that only proportional control is activated, i.e. $k_i=0$, the equation (4) can be simplified as

$$|T_2(s)| = \frac{Kk_p}{\sqrt{(L\omega)^2 + (Kk_p)^2}} \quad (5)$$

It is well known that the bandwidth is defined as the frequency where the magnitude attenuation is -3 dB. If the expected initial bandwidth ω_{ib} is fixed, the proportional parameter k_p can be calculated from (5) as

$$k_p = \frac{L\omega_{ib}}{K} \quad (6)$$

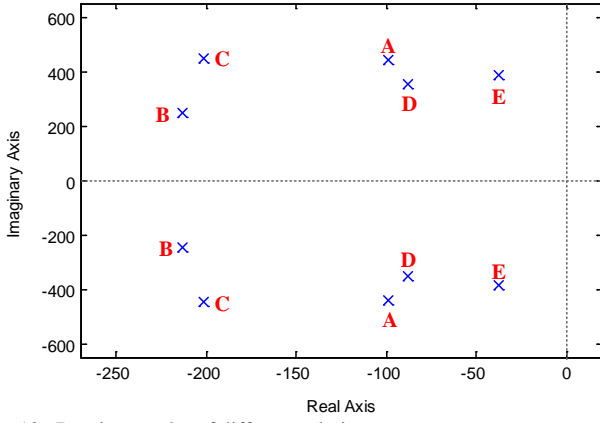**Step 2.** Assuming that the integral control with the simple feedback term is integrated into the proportional control, the magnitude-frequency characteristic can be expressed by (4). If the expected final bandwidth ω_{fb} is decided, the integral parameter k_i can be calculated from (4) as

$$k_i = \frac{(\omega_{fb} - \omega_0)}{K}(\sqrt{2(\omega_{fb}L)^2 - K^2k_p^2} - \omega_{fb}L) \quad (7)$$

Step 3. Evaluate the system stability by confirming that the closed-loop system has no right-half-plane poles.

In this paper, the expected initial and final bandwidths are set to 1 kHz and 1.1 kHz respectively and, thus, the controller parameters can be calculated by the three-step method, yielding $k_p = 0.2$ and $k_i = 80$. Then, the close-loop poles ($-6276.3 - 22.7j$ and $423.7 - 336.7j$) are located on the left half plane, which indicates the system is stable.

C. Practical implementation of the term 'j'

In a single-phase grid-connected inverter system, it is very difficult to implement the term "j" in Fig. 7. However, the total harmonic distortion of the grid current should be less than 5%, as specified in IEEE Std.929-2000 and IEEE Std.1547. Therefore, in most cases, the fundamental component is dominant, and current harmonics are small enough to neglect. In this case, the term "j" can be physically implemented by considering the unity amplitude and 90 degrees phase shift at the fundamental frequency.

Physical implementations of the complex number 'j' can be classified into two main methods: the time-domain and frequency-domain based methods.

The simplest time-domain method is shown in Fig. 10, where the delay, that is 5 ms, is equivalent to the complex number 'j' from the viewpoint of the unity gain and 90 degrees phase shift features.

Fig. 10. Single-phase natural frame control with SR

On the other hand, from the fundamental frequency point of view, 'j' can be implemented in the frequency domain

with characteristics of the unity gain and 90 degrees phase shift at the fundamental frequency by low pass filters or all pass filters, as listed in Table I.

It is our worth to note that the proposed controller will be equivalent to the well-known PR controller [28-30], if the first-order low pass filter is used, as shown in Fig. 11. Therefore PR controller is just a special case of the proposed general unified controller.

TABLE I. PRACTICAL FILTERS FOR 'J '

	Low Pass Filter	All Pass Filter
First order	$\dfrac{\omega_0}{s}$	$\dfrac{-s + \omega_0}{s + \omega_0}$
Second order	$\dfrac{k\omega_0^2}{s^2 + k\omega_0 s + \omega_0^2}$	$\dfrac{s^2 - k\omega_0 s + \omega_0^2 + k\omega_0^2}{s^2 + k\omega_0 s + \omega_0^2 + k\omega_0^2}$

Fig. 11. Proposed controller when "j" is implemented with ω_0/s

We emphasize that the controller in SubSection C is not mathematically equivalent to the controller in Fig. 7 in the entire frequency range, so the transient responses are different, as shown in the following SubSection. However, the characteristics are the same at the fundamental frequency to achieve the zero steady-state error for the single-phase grid-connected inverter.

D. Performance Evaluation

As discussed in the previous section, there are five alternative implementation methods of the proposed control. The performance comparison of the five alternative methods will be shown in this SubSection. The comparison criteria used will be the dynamic response, stability and the total harmonic distortion (THD) of the grid current.

It is well know that the system closed-loop poles are useful to study the system stability and transient response. In general, the system is stable if all the poles are located in the left half plane. When the left-half-plane poles are far away from the imaginary axis the dynamic response became faster.

Fig. 12 shows the dominant poles of the closed-loop system with different solutions. All the methods can ensure the system stability due to the dominant poles located in the left half pane. In addition, it can be observed that three solutions (A, D and E) show slower dynamic response, while the other two solutions (B and C) have faster dynamic response due to their dominant poles further away from the imaginary axis.

Fig. 12. Dominant poles of different solutions

TABLE II
PERFORMANCE EVALUATON

	Dominant poles	$|D(s)|$ @150Hz
Delay 5ms (Solution A)	-98.8+441i -98.8-441i	0.0246
$\dfrac{\omega_0}{s}$ (Solution B)	-213+245i -213-245i	0.0235
$-\dfrac{s-\omega_0}{s+\omega_0}$ (Solution C)	-202+445i -202-445i	0.0276
$\dfrac{k\omega_0^2}{s^2+k\omega_0 s+\omega_0^2}$ (Solution D)	(k=1) -87.9+354i -87.9-354i	(k=1) 0.0243
	(k=10) -209+273i -209-273i	(k=10) 0.0239
$\dfrac{s^2-k\omega_0 s+\omega_0^2+k\omega_0^2}{s^2+k\omega_0 s+\omega_0^2+k\omega_0^2}$ (Solution E)	(k=1) -37.8+386i -37.8-386i	(k=1) 0.0232
	(k=10) -158+453i -158-453i	(k=10) 0.0278

On the other hand, the system disturbance rejection characteristic shows the effect of the grid voltage harmonics on the grid current, as following:

$$D(s)=\frac{I_g(s)}{U_g(s)}=-\frac{(s-j\omega_0)(T_d s+1)}{[LT_d s^2+(RT_d+L)s+R](s-j\omega_0)+KM(s)}$$
(8)

Note that the harmonic components of the grid voltage mainly consist of a low-order harmonics, and their magnitude may tend to be lower as their frequency increases. Therefore, only the third (150Hz) harmonic of the grid voltage is considered as an example in the following theoretical performance evaluation.

Te system disturbance rejection characteristic for different solutions (k=1) is depicted in Fig. 13. It can be observed that solution C is sensitive to low-order harmonics of the grid voltage, while the other three solutions (A, B, D and E) have better grid disturbance rejection capability due to their smaller gains of $\left|I_g(s)/U_g(s)\right|$.
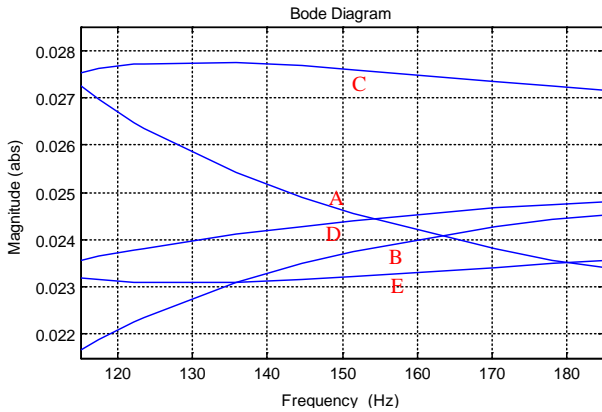
Fig. 13. Disturbance rejection characteristic $\left|I_g(s)/U_g(s)\right|$

Table II summarizes the system disturbance rejection characteristic for the low-order harmonic frequencies and the dominant poles as well. It can be concluded that Solutions B and C are better from the dynamic response viewpoint. On the other hand, all of them have similar steady-state performances, while solutions A, B, D and E are slightly superior in terms of grid disturbance rejection capability.

Notice that the system performances of solutions D and E are dependent on the cutoff frequency of filters, more specifically, the coefficient "k". From Table II, it can be observed that the system performance tends to be better for Solution D and Solution E. Therefore, 'k' should be carefully designed for better performance in practical applications.

Another consideration that should be noted is that the zero steady-state error is achieved on condition that the grid frequency is time-invarying. However, in practical situations the grid frequency may suffer fluctuations, such as in case of weak grids or islanded MicroGrids [1]. In this case, it is recommended that the proposed controller should be adaptively adjusted. For example, the buffer length will be adaptively changed with the frequency when using solution A. Furthermore, some other possible solutions have been reported in [31], which are beyond the scope of this paper.

IV. PERFORMANCE EVALUATION AND DISCUSSION

In order to verify the effectiveness of the proposed control strategy, the simulation and experimental tests are carried out based on a single-phase grid-connected inverter. The system consists of an H-bridge with four IGBTs and two split inductors ($L_1=L_2=3$mH). The dc-link voltage of the inverter is fed with a DC power supply (rated 200V). The system output is connected to the grid through a 220/110-V 3-kVA single-phase transformer. The grid current reference is 5A. The inverter is controlled by a 32-bit fixed-point 150MHz TMS320F2812 DSP platform, and the switching frequency and sampling frequency is set to 10 kHz. In this section, we will provide the performance evaluation results of the proposed control with the five aforementioned alternative implementations, in contrast with the conventional PI controller.
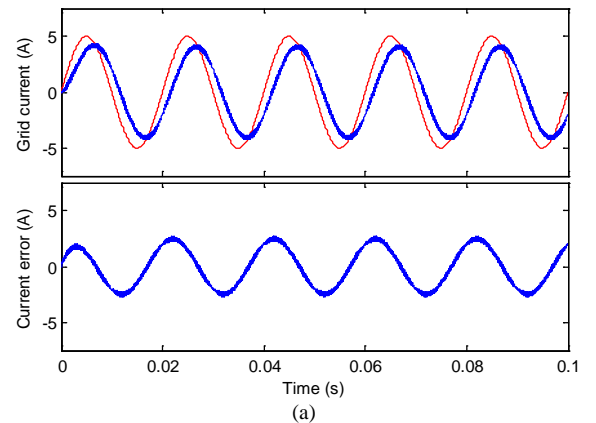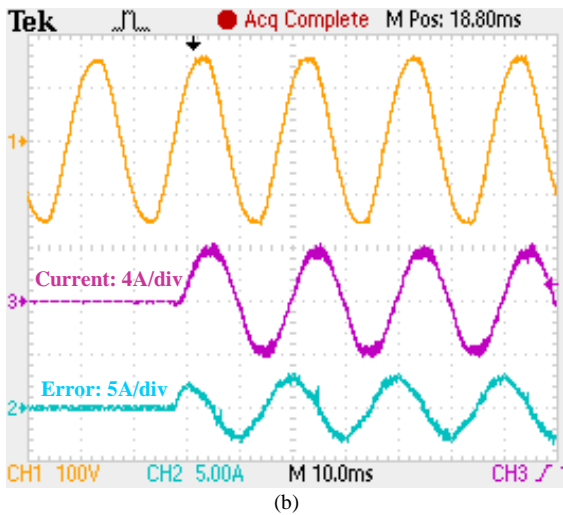
Fig. 14. Test results with PI control. (a) Simulation result. (b) Experimental results.

Fig. 14 (a) shows the time-domain simulation results. It can be clearly observed that the grid current has steady-state errors in both amplitude and phase when using the conventional PI control. On the other hand, the corresponding experimental results are shown in Fig. 14 (b), which are in good agreement with the simulation results. However, the grid current presents a slight distortion, mainly resulting from the distorted grid voltage.

(a)

(b)
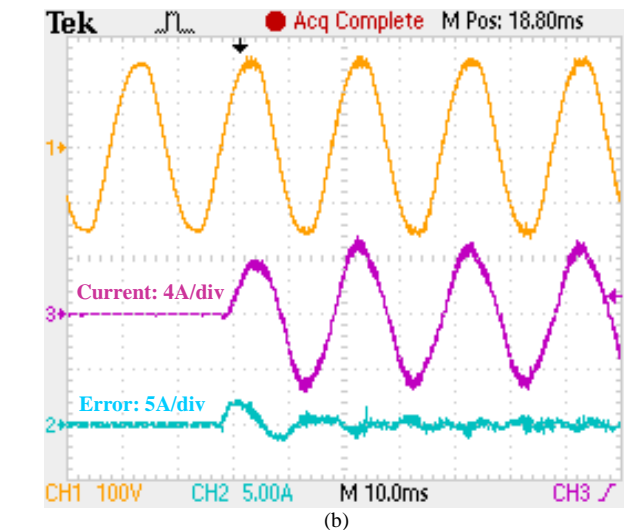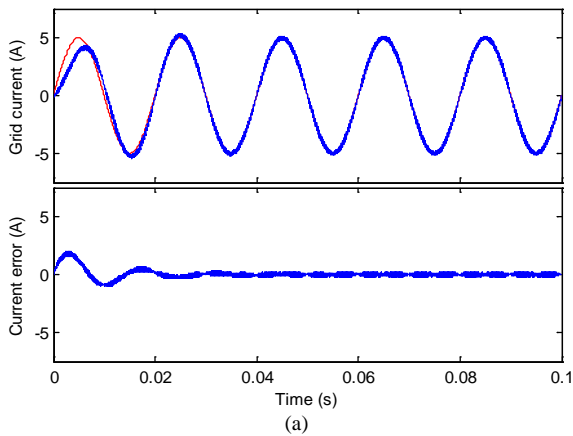
Fig. 15. Test results with Solution A. (a) Simulation result. (b) Experimental results.

The time-domain simulation results in solution A (see Table II) is shown in Fig. 15. It can be observed that the grid

current tracks its reference with zero steady-state error after the startup transient within one and a half cycle. In good agreement with the theoretical analysis in the previous sections, there is a 70.2 Hz decaying, oscillating response, which is mainly dependent on the imaginary parts of the dominant, poorly damped low-frequency poles (see Table II). On the other hand, the experimental results are similar of those from the simulation ones, except for the small current distortion, which is due to the background harmonics of the grid voltage.

Fig. 16 shows the simulation and experimental results when using solution B. The zero steady-state error tracking of the current reference can be observed. Note that the transient response of Solution B is about 15 ms, being faster than the solution A. The reason of this is that the dominant poles of solution B are more far from the imaginary axis than those of solution A (see Table II). Therefore, it can be concluded that the steady-state performance is almost the same for both solutions. However, the dynamic performance of solution B is better than the solution A, which is in agreement with the theoretical analysis presented in Table II.
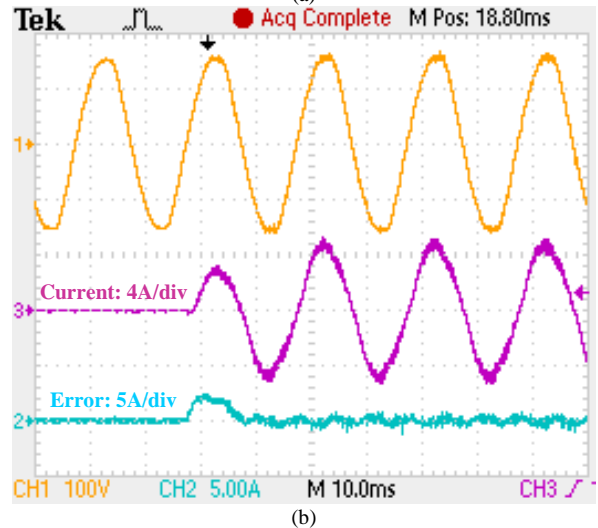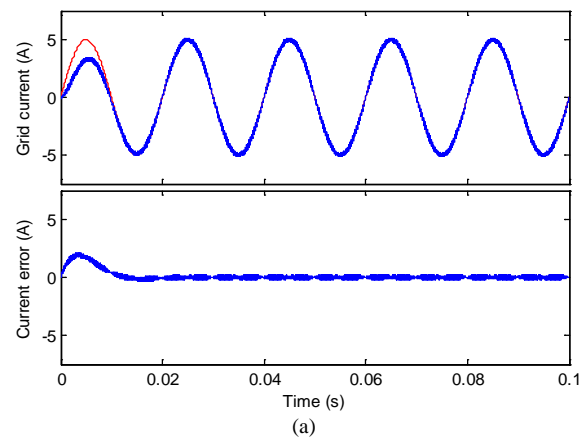

(a)

(b)

Fig. 16. Test results with Solution B. (a) Simulation result. (b) Experimental results.

Fig. 17 shows the simulation and experimental results of solution C. As can be derived from Table II, the transient response time of solution C is almost the same as solution B. The reason for this is that the distance of their dominant poles are similarly far from the imaginary axis. On the other hand, there is a 70.8 Hz decaying, oscillating response, which is mainly dependent on the imaginary parts of the dominant, but poorly damped low-frequency poles.
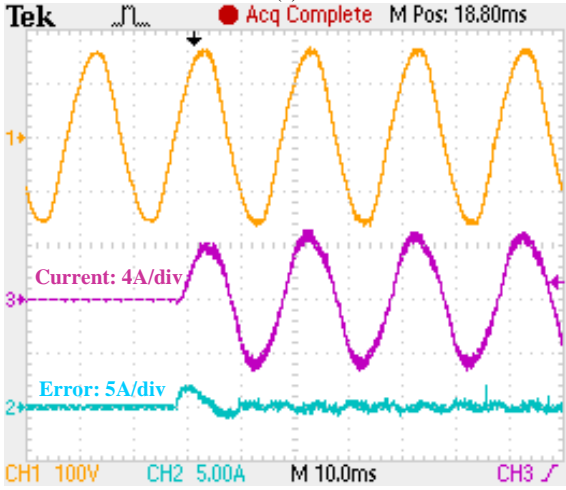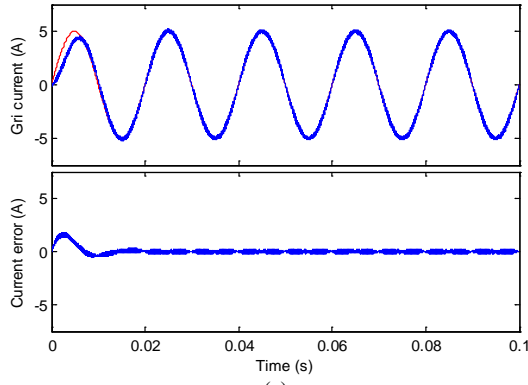
Fig. 17. Test results with Solution C. (a) Simulation result. (b) Experimental results.
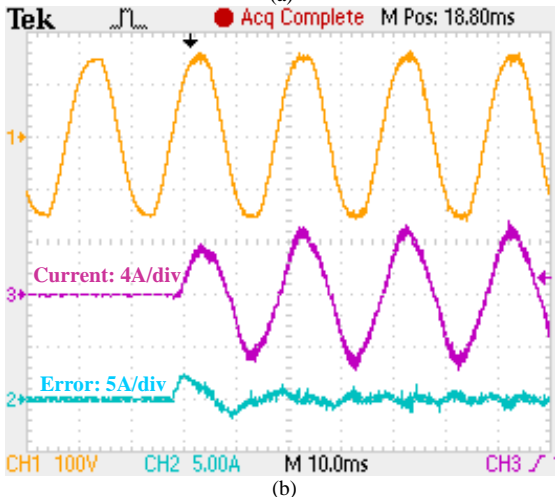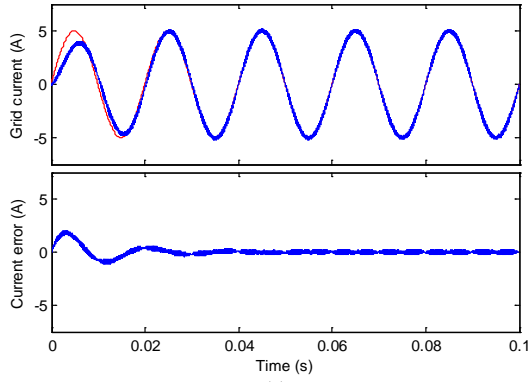

Fig. 18. Test results with Solution D (k=1). (a) Simulation result. (b) Experimental results.
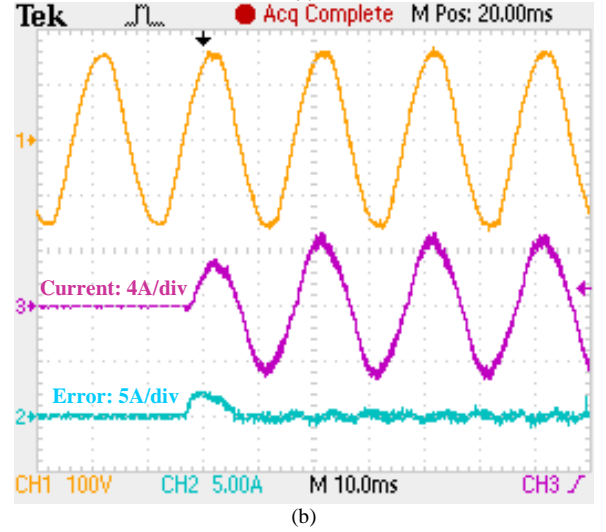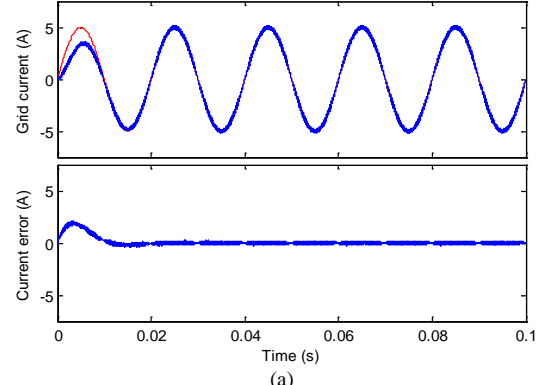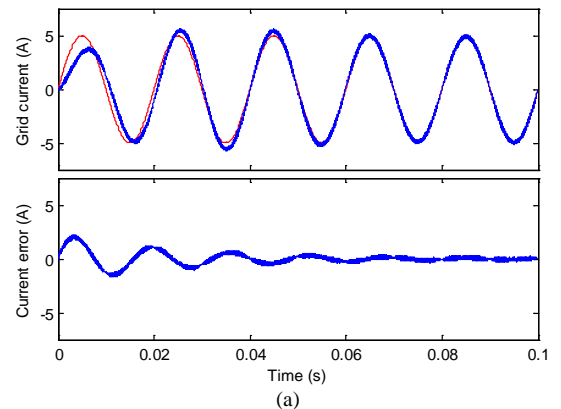

Fig. 19. Test results with Solution D (k=10). (a) Simulation result. (b) Experimental results.

Fig. 18 and Fig. 19 show the simulation and experimental results of solution D for different coefficients (k=1 and k=10). It can be observed that the steady-state performance is similar in both cases. However, the transient response of solution D would be better for higher gain of k, as expected from Table II.

The simulation and experimental results of solution E for different coefficients (k=1 and k=10) are shown in Fig. 20 and Fig. 21. It can be observed that the steady-state performance is similar for both cases. However, the transient response of solution E for k=1 is the slowest one among all aforementioned solutions, which is in agreement with the theoretical analysis presented in Table II. On the other hand, the transient response is better for higher gain of k=10. The reason is that the dominant poles for k=10 are far away from the imaginary axis than those for k=1 (see Table II).
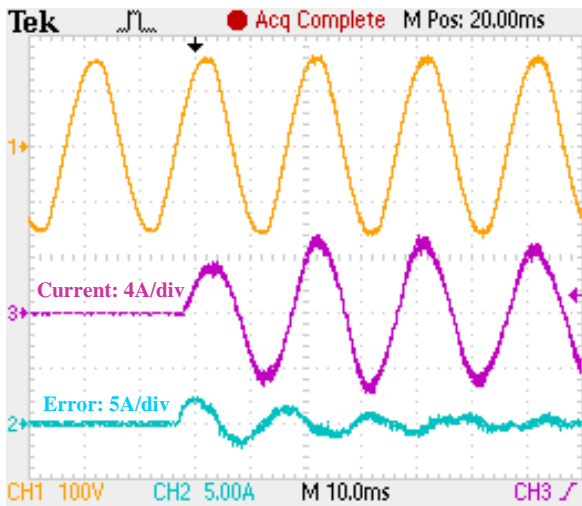

(a)

Fig. 20. Test results with Solution E (k=1). (a) Simulation result. (b) Experimental results.
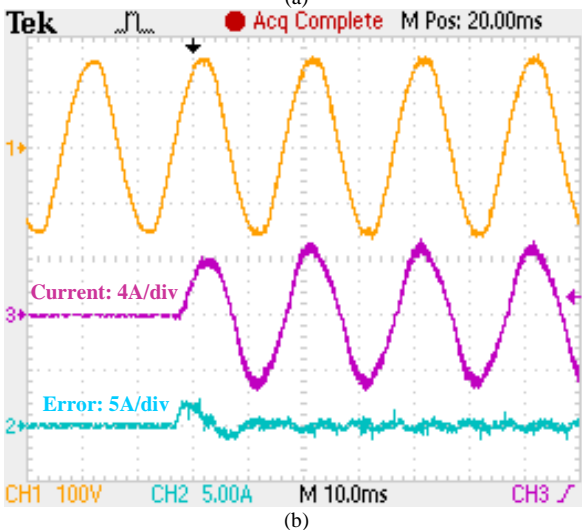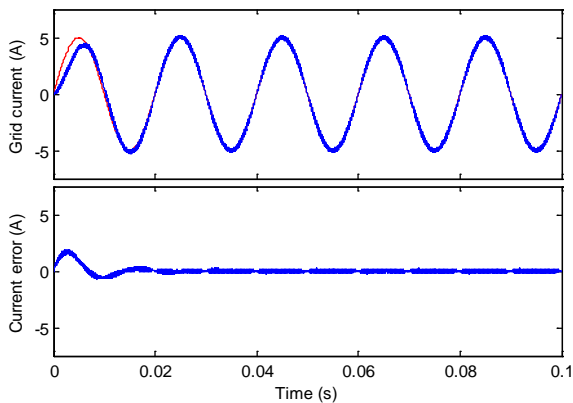

Fig. 21. Test results with Solution E (k=10). (a) Simulation result. (b) Experimental results.

Table III summarizes the performance comparison between all the cases. In good agreement with the theoretical analysis in Table II, solutions A, D (k=1), and E (k=1) presents slower dynamic response, while solutions B, C, D (k=10), and E (k=10) show faster dynamic response. On the other hand, all of these solutions have similar steady-state error performances, while solutions C and E (k=10) are not preferred from the viewpoint of grid disturbance rejection capability.

TABLE III
PERFORMANCE COMPARISON

	Response time	Current THD
Delay 5ms (Solution A)	30ms	3.8%
$\dfrac{\omega_0}{s}$ (Solution B)	15ms	3.8%
$-\dfrac{s-\omega_0}{s+\omega_0}$ (Solution C)	15ms	4.4%
$\dfrac{k\omega_0^2}{s^2+k\omega_0 s+\omega_0^2}$ (Solution D)	30ms(k=1)	3.8%(k=1)
	15ms(k=10)	3.7% (k=10)
$\dfrac{s^2-k\omega_0 s+\omega_0^2+k\omega_0^2}{s^2+k\omega_0 s+\omega_0^2+k\omega_0^2}$ (Solution E)	30ms(k=1)	3.6% (k=1)
	15ms(k=10)	4.5% (k=10)

V. CONCLUSION

This paper has presented how a simple feedback terms is integrated into the conventional PI controller to eliminate the steady-state error of the grid current at the fundamental frequency without any other complex control algorithms. Five alternative implementation methods of the proposed control are comparatively evaluated from the viewpoint of the steady-state and dynamic responses. Theoretical analysis, simulation and experimental results are in good agreement, which indicates five alternative methods can achieve the zero steady-state error control for the single-phase PV inverter. But their dynamic responses and grid disturbance rejection performances are slightly different. Therefore, a careful selection among five alternative methods should be needed for the high performance control of the single-phase grid-connected inverters. It is recommended that Solution B and D would be good choices in terms of the steady-state and dynamic performances. It should be note that, the total harmonic distortion of the grid current is generally less than 5%, as specified in IEEE Std. 929-2000 and IEEE Std.1547. Therefore, in most cases, the fundamental component is dominant, and current harmonics are relatively small. But when the reference is very small, the harmonic in the current might be comparable to the fundamental. In this case, the proposed control should be modified to control the harmonic component. It needs a comprehensive and systematic investigation, which will be the subject of our future research.

REFERENCES

[1] J. M. Guerrero, J. C. Vasquez, J. Matas, L. G. de Vicuna, and M. Castilla, "Hierarchical control of droop-controlled AC and DC microgrids—A general approach towards standardization," *IEEE Trans. Ind. Electron.,* vol. 58, no. 1, pp. 158–172, Jan. 2011.

[2] Y. A.-R. I.Mohamed and A. Radwan, "Hierarchical control system for robust micro-grid operation and seamless mode-transfer in active distribution systems," *IEEE Trans. Smart Grid*, vol. 2, no. 2, pp. 352–362, Jun. 2011.

[3] T. L. Vandoorn, B. Renders, L. Degroote, B. Meersman, and L. Vandevelde, "Active load control in islanded microgrids based on the grid voltage," *IEEE Trans. Smart Grid*, vol. 2, no. 1, pp. 139–151, Mar. 2011.

[4] Y. Li and Y. W. Li, "Power management of inverter interfaced autonomous microgrid based on virtual frequency-voltage frame," *IEEE Trans. Smart Grid*, vol. 2, no. 1, pp. 30–40, 2011.

[5] K. T. Tan, X. Y. Peng, P. L. So, Y. C. Chu, and M. Z. Q. Chen, "Centralized control for parallel operation of distributed generation inverters in microgrids," *IEEE Trans. Smart Grid*, vol. 3, no. 4, pp. 1977–1987, Dec. 2012.

[6] P. C. Loh, D. Li, Y. K. Chai, and F. Blaabjerg, "Autonomous operation of hybrid microgrid with AC and DC subgrids," *IEEE Trans. on Power Electron.*, vol. 28, no. 5, pp. 2214-2223, May 2013.

[7] R. Majumder, "A hybrid microgrid with dc connection at back to back converters," *IEEE Trans. Smart Grid.*, vol. 5, no. 1, pp. 251–259, Jan. 2014.

[8] J. He, Y. W. Li, D. Bosnjak, and B. Harris, "Investigation and active damping of multiple resonances in a parallel-inverter-based microgrid," *IEEE Trans. Power Electron.*, vol. 28, no. 1, pp. 234–246, Jan. 2013.

[9] J. Sun, "Impedance-based stability criterion for grid-connected inverters," *IEEE Trans. Power Electron.*, vol. 26, no. 11, pp. 3075–3078, Nov. 2011.

[10] W. Li, X. Ruan, D. Pan, and X. Wang, "Full-feedforward schemes of grid voltages for a three-phase LCL-type grid-connected inverter," *IEEE Trans. Ind. Electron.*, vol. 60, no. 6, pp. 2237–2250, Jun. 2013

[11] M. A. Herran, J. R. Fischer, S. A. Gonzalez, M. G. Judewicz, and D. O. Carrica, "Adaptive dead-time compensation for grid-connected PWM inverters of single-stage PV systems," *IEEE Trans. Power Electron.*, vol. 28, no. 6, pp. 2816–2825, Jun. 2013.

[12] Z. Yao and L. Xiao, "Two-switch dual-buck grid-connected inverter with hysteresis current control," *IEEE Trans. Power Electron.*, vol. 27, no. 7, pp. 3310–3318, Jul. 2012.

[13] W. Fengjiang, S. Bo, Z. Ke, and S. Li, "Analysis and solution of current zero-crossing distortion with unipolar hysteresis current control in grid-connected inverter," *IEEE Trans. Ind. Electron.*, vol. 60, no. 10, pp. 4450– 4457, Oct. 2013.

[14] Y. Chen and K. M. Smedley, "One cycle controlled three-phase grid-connected inverters and their parallel operation," *IEEE Trans. Ind. Appl.*, vol. 44, no. 2, pp. 663–671, Mar./Apr. 2008.

[15] Q. Zeng and L. Chang, "An advanced SVPWM-based predictive current controller for three-phase inverters in distributed generation systems," *IEEE Trans. Ind. Electron.*, vol. 55, no. 3, pp. 1235–1246, Mar. 2008.

[16] V. Yaramasu and B. Wu, "A model predictive decoupled active and reactive power control for high power grid-connected four-level diode clamped inverters," *IEEE Trans. Ind. Electron.*, vol. 61, no. 7, pp. 3407–3416,

[17] C. Meza, D. Biel, D. Jeltsema, and J. Scherpen, "Lyapunov-based control scheme for single-phase grid-connected PVcentral inverters," *IEEE Trans. Control Syst. Technol.*, vol. 20, no. 2, pp. 520–528, Mar. 2012.

[18] R. Zhang, M. Cardinal, P. Szczesny, and M. Dame, "A Grid simulator with control of single-phase power converters in D-Q rotating frame," in *Proc. IEEE Power Electron. Spec. Conf.*, 2002, pp. 1431-1436.

[19] R. Y. Kim, S. Y. Choi, and I. Y. Suh, "Instantaneous control of average power for grid tie inverter using single phase D-Q rotating frame with all pass filter," in *Proc. IEEE Ind. Electron. Conf.*, Busan, Korea, Nov. 2004, pp. 274-279.

[20] M. Milanés-Montero, E. Romero-Cadaval, A. Rico de Marcos, V. Minambres-Marcos,and F. Barrero-Gonzalez, "Novel method for synchronization to disturbed three-phase and single-phase systems," in *Proc. IEEE Ind. Electron. Conf.*, Vigo, Spain, 2007, pp. 860-865.

[21] S. Chung, "Steady-state error minimization technique for single-phase PWM inverters," *Electronics Letters*, vol. 38, no. 22, pp. 1378–1380, Oct. 2002.

[22] Z. R. Ivanovic, E. M.Adžić, M. S. Vekić, S. U. Grabić, N. L. Čelanović, and V. A. Katić, "HIL evaluation of power flow control strategies for energy storage connected to smart grid under unbalanced conditions," *IEEE Trans. Power Electron.*, vol. 27, no. 11, pp. 4699–4710, Nov. 2012.

[23] S. Adhikari, F. Li, "Coordinated V-f and P-Q control of solar photovoltaic generators with MPPT and battery storage in microgrids," *IEEE Trans. Smart Grid*, vol. 5, no. 3, pp. 1270–1281, May 2014.

[24] X. Wang, W. Freitas, and W. Xu, "Dynamic non-detection zones of positive feedback anti-islanding methods for inverter-based distributed generators," *IEEE Trans. Power Del.*, vol. 26, no. 2, pp. 1145–1155, Apr. 2011.

[25] D. Yazdani, A. Bakhshai, G. Joos, and M. Mojiri, "A nonlinear adaptive synchronization technique for grid-connected distributed energy sources," *IEEE Trans. Power Electron.*, vol. 23, no. 4, pp. 2181–2186, Jul. 2008.

[26] H. F. Xiao, X. P. Liu, and K. Lan, "An Optimized Full Bridge Transformerless PV Grid-Connected Inverter With Low Conduction Loss and Low Leakage Current," *IET Power Electron.*, vol. 7, no. 4, pp. 1008-1015, Feb. 2014.

[27] R. Turner, S. Walton, and R. Duke, "Stability and bandwidth implications of digitally controlled grid-connected parallel inverters," *IEEE Trans. Ind. Electron.*, vol. 57 no. 11, pp. 3685–3694, Nov. 2010.

[28] R. Teodorescu, F. Blaabjerg, M. Liserre, and P. C. Loh, "Proportional resonant controllers and filters for grid-connected voltage-source converters," *Proc. Inst. Elect. Eng.—Elect. Power Appl.*, vol. 153, no. , pp. 750–762, Sep. 2006.

[29] A. G. Yepes, F. D. Freijedo, J. Doval-Gandoy, O. Lopez, J. Malvar, and P. Fernandez-Comesana, "Effects of discretization methods on the performance of resonant controllers," *IEEE Trans. Power Electron.*, vol. 25, no. 7, pp. 1692–1712, Jul. 2010.

[30] A. G. Yepes, F. D. Freijedo, O . Lopez, and J. Doval-Gandoy, "High performance digital resonant controllers implemented with two integrators," *IEEE Trans. Power Electron.*, vol. 26, no. 2, pp. 563–576, Feb. 2011.

[31] F. D. Freijedo, "Contributions to grid-synchronization techniques for power electronic converter," Ph.D. dissertation, Dept. Electron. Technol., Vigo Univ., Vigo, Spain, Jun. 2009.

X. Guo (M' 10-SM' 14) received the B.S. and Ph.D. degrees in electrical engineering from Yanshan University, Qinhuangdao, China, in 2003 and 2009, respectively.

He has been a Postdoctoral Fellow with the Laboratory for Electrical Drive Applications and Research (LEDAR), Ryerson University, Toronto, ON, Canada. He is currently an associate professor with the Department of Electrical Engineering, Yanshan University, China. He has authored/coauthored more than fifty technical papers, in addition to nine patents. His current research interests include high-power converters and ac drives, electric vehicle charging station, and renewable energy power conversion systems.

Dr. Guo is a Senior Member of the IEEE Power Electronics Society and IEEE Industrial Electronics Society. He is an active Referee for IEEE Transactions on Industrial Electronics and IEEE Transactions on Power Electronics.

Josep M. Guerrero (S'01-M'04-SM'08-F'15) received the B.S. degree in telecommunications engineering, the M.S. degree in electronics engineering, and the Ph.D. degree in power electronics from the Technical University of Catalonia, Barcelona, in 1997, 2000 and 2003, respectively. Since 2011, he has been a Full Professor with the Department of Energy Technology, Aalborg University, Denmark, where he is responsible for the Microgrid Research Program. From 2012 he is a guest Professor at the Chinese Academy of Science and the Nanjing University of Aeronautics and Astronautics; from 2014 he is chair Professor in Shandong University; and from 2015 he is a distinguished guest Professor in Hunan University.

His research interests is oriented to different microgrid aspects, including power electronics, distributed energy-storage systems, hierarchical and cooperative control, energy management systems, and optimization of microgrids and islanded minigrids. Prof. Guerrero is an Associate Editor for the IEEE TRANSACTIONS ON POWER ELECTRONICS, the IEEE TRANSACTIONS ON INDUSTRIAL ELECTRONICS, and the IEEE Industrial Electronics Magazine, and an Editor for the IEEE TRANSACTIONS on SMART GRID and IEEE TRANSACTIONS on ENERGY CONVERSION. He has been Guest Editor of the IEEE TRANSACTIONS ON POWER ELECTRONICS Special Issues: Power Electronics for Wind Energy Conversion and Power Electronics for Microgrids; the IEEE TRANSACTIONS ON INDUSTRIAL ELECTRONICS Special Sections: Uninterruptible Power Supplies systems, Renewable Energy Systems, Distributed Generation and Microgrids, and Industrial Applications and Implementation Issues of the Kalman Filter; and the IEEE TRANSACTIONS on SMART GRID Special Issue on Smart DC Distribution Systems. He was the chair of the Renewable Energy Systems Technical Committee of the IEEE Industrial Electronics Society. In 2014 he was awarded by Thomson Reuters as Highly Cited Researcher, and in 2015 he was elevated as IEEE Fellow for his contributions on "distributed power systems and microgrids."